SERI/TP-257-3603
UC Category: 261
DE89009512

A Comparison of Two- and Three-Dimensional S809 Airfoil Properties for Rough and Smooth HAWT Rotor Operation

W. D. Musial
C. P. Butterfield
M. D. Jenks

February 1990

Prepared for the
9th ASME Wind Energy Symposium
New Orleans, Louisiana
14-18 January, 1990

Prepared under Task No. WE011001

Solar Energy Research Institute
A Division of Midwest Research Institute

1617 Cole Boulevard
Golden, Colorado 80401-3393

Prepared for the
U.S. Department of Energy
Contract No. DE-AC02-83CH10093

NOTICE

Printed in the United States of America
Available from:
National Technical Information Service
U.S. Department of Commerce
5285 Port Royal Road
Springfield, VA 22161

Price: Microfiche A01
Printed Copy A02

Codes are used for pricing all publications. The code is determined by the number of pages in the publication. Information pertaining to the pricing codes can be found in the current issue of the following publications which are generally available in most libraries: *Energy Research Abstracts (ERA)*; *Government Reports Announcements* and Index (*GRA* and I); *Scientific and Technical Abstract Reports (STAR)*; and publication NTIS-PR-360 available from NTIS at the above address.

A Comparison of Two- and Three-Dimensional S809 Airfoil Properties for Rough and Smooth HAWT Rotor Operation

W. D. Musial
C. P. Butterfield
M. D. Jenks

Solar Energy Research Institute
1617 Cole Blvd.
Golden, Colorado 80401

ABSTRACT

At the Solar Energy Research Institute (SERI), we carried out tests to measure the effects of leading-edge roughness on an S809 airfoil using a 10-m, three-bladed, horizontal-axis wind turbine (HAWT). The rotor employed a constant-chord (.457 m) blade geometry with zero twist. Blade structural loads were measured with strain gages mounted at 9 spanwise locations. Airfoil pressure measurements were taken at the 80% spanwise station using 32 pressure taps distributed around the airfoil surface. Detailed inflow measurements were taken using nine R.M. Young Model 8002 propvane anemometers on a vertical plane array (VPA) located 10 m upwind of the test turbine in the prevailing wind direction.

The major objective of this test was to determine the sensitivity of the S809 airfoil to roughness on a rotating wind turbine blade. We examined this effect by comparing several parameters. We compared power curves to show the sensitivity of whole rotor performance to roughness. We used pressure measurements to generate pressure distributions at the 80% span which operates at a Reynolds number (Re) of 800,000. We then integrated these distributions to determine the effect of roughness on the section's lift and pressure-drag coefficients. We also used the shapes of these distributions to understand how roughness affects the aerodynamic forces on the airfoil. We also compared rough and smooth wind tunnel data to the rotating blade data to study the effects of blade rotation on the aerodynamic behavior of the airfoil below, near, and beyond stall.

INTRODUCTION

Leading-edge roughness on wind turbine blades is a universal problem that affects most manufacturers and developers of wind turbines. It has contributed significantly to lower energy production, spoiling wind turbine control algorithms and making loads more difficult to predict.

The majority of HAWTs use aerodynamic stall to regulate peak power and loads. Consequently, most wind turbines experience stall during normal operating conditions and over significant portions of the blade. Operating airfoils in and beyond stall has lead to several problems. First, there are very few wind tunnel data for airfoil performance beyond the maximum lift coefficient (C_{lmax}). Second, it is not yet clear how the three-dimensional (3-D) rotational effects change the airfoil section properties in the stalled region. Because wind turbines commonly operate at very high angles of attack (AOA), load predictions are often based on uncertain airfoil performance data, which contributes to significant errors in estimates of peak performance.

When airfoil surfaces become roughened by insects and dirt, this uncertainty is increased. Blade surface roughness has been observed to decrease the peak power output of stall-controlled wind turbines by as much as 40% (1). Most of the degradation can usually be attributed to premature airfoil stalling, which lowers C_{lmax}. This can greatly inhibit the accuracy of wind turbine performance predictions, especially when the degree of roughness is constantly changing because of uncontrolled environmental factors.

The effects of roughness on HAWT airfoils are most commonly quantified by examining the influence on the power curve of a particular rotor. This method is very accurate and reliable for determining the impact on energy capture for a given HAWT configuration, but it does not provide much information about changes to the aerodynamic properties of the airfoil. If two-dimensional (2-D) wind tunnel data exist for a rough airfoil, they may be used to predict performance degradation in the sub-stall regions; still, there has been little success with attempts to accurately predict performance in the stall or post-stall regions using 2-D data. Measurements taken directly off the rotating airfoil will give the clearest picture of how roughness affects the airfoil properties.

The problem is that the stalled airfoil performance on a rotating blade appears to be modified by 3-D flow effects. For example, Madsen et al. (2) hypothesize that the lift curve slope and C_{lmax} appear to be reduced on outboard blade sections, while inboard C_{lmax} appears to be increased. It is common for wind turbine designers to underestimate peak performance and

loads. Although part of the cause is poor airfoil data, as mentioned above, there are additional effects caused by blade rotation.

To understand the physics controlling these stall-related phenomena, SERI (sponsored by the U. S. Department of Energy) has begun a detailed measurement program on a 10-m, three-bladed HAWT. This multifaceted test, known as the Combined Experiment (3), has produced measurements of far-field atmospheric boundary layer, near-field inflow using a VPA and high-frequency response anemometry, airfoil pressure distributions at 80% radius, video images of surface flow patterns, blade loads at nine spanwise locations, and turbine structural loads. We are using this detailed data set to study a wide variety of atmospheric and aerodynamic phenomena on a rotating blade.

At SERI, we have also recently developed two new airfoil families. These airfoils are specially designed to control peak power on wind turbines and should eliminate most of the shortcomings found in conventional aircraft airfoils. One of the major design objectives was to make the airfoil properties insensitive to roughness (4,5). The Combined Experiment test turbine offered a convenient opportunity to test one of the special-purpose airfoils, and at the same time verify its leading-edge roughness sensitivity characteristics on a rotating blade. We chose the S809 airfoil for this experiment due to its relatively large experimental 2-D data base.

TEST METHOD

Test Turbine

We performed roughness tests during the Combined Experiment test program using the 10-m-diameter, three-bladed, downwind test turbine. This machine is equipped with full-span pitch control that is manually operated during the testing to allow fixed-pitch (stall-controlled) operation at any pitch angle desired. The blade had a constant 0.45-m (18-in) chord with zero twist, and they rotated at a constant 72 rpm. A schematic of this turbine is shown in Figure 1.

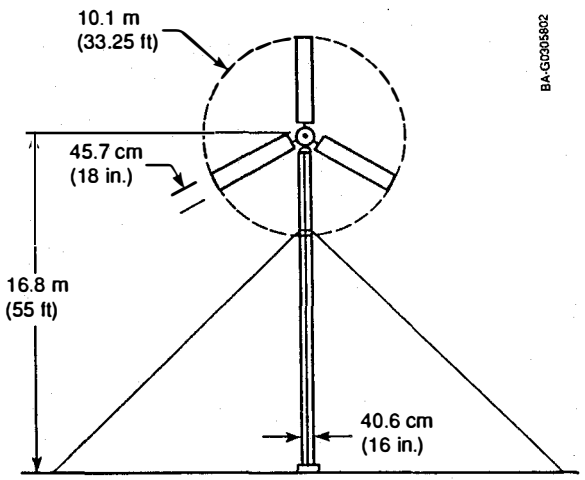

Windstream 33 Characteristics	
Induction generator rating	20 kW
Induction generator speed range	1800-1860 rpm
Gearbox ratio	25.1:1
Rotor speed	74.1 rpm
Rotor diameter	33.25 ft
Rotor solidity	0.0615
Blade chord	1.5 ft
Power coefficient, Max ($C_{P\ MAX}$)	0.38°
Tip speed ratio at $C_{P\ MAX}$	5.25°
Wind speed at $C_{P\ MAX}$	17.0 mph
System efficiency at $C_{P\ MAX}$	83%
Output power at VW = 24 mph	15 kW*
Rotor coning angle	3-1/2°
Razor/Nacelle assembly wt.	2,589 lb.
Drive axis height	55 ft
Tower section	16.0 in./0 dia, 3/8 in. wall
Guy base	80 ft

*Predicted

Fig. 1 Layout of the Combined Experiment test machine

Leading-Edge Roughness

Most airfoil roughness problems experienced by HAWTs have been caused primarily by insects accumulating on the surface near the leading edge of the blade. The distribution is generally non-uniform, with larger particle sizes and particle densities distributed near the leading edge and rapidly declining toward the trailing edge.

The NACA standard roughness was created to simulate the typical roughness distribution experienced by aircraft. This standard consists of a uniform distribution of particles between the leading-edge and the 8% chord line on the upper and lower surfaces of the airfoil (6). Particle size is defined by the non-dimensional ratio of the particle diameter (k) divided by the chord length (c). The k/c value for the NACA standard roughness is 0.00046, which corresponds to grit sizes of 0.21 mm (0.0083 in.) for the Combined Experiment rotor.

However, operating conditions for wind turbines are quite different than for aircraft. Wind turbines operate closer to the ground, at lower Re, and are cleaned less frequently. Consequently, the NACA standard roughness is not as severe as the actual accumulation of insects observed by the authors. To realistically test rough airfoil performance on the S809, it was necessary to create a roughness pattern that was more appropriate for wind turbine applications.

A new "simulated insect" roughness was then developed and applied to all three blades over the outer 3.35 m (11 ft). Coarse grit particles, ranging in size from 0.5 to 1.0 mm (0.020 to 0.040 in.) were distributed onto a 20.3-cm (8-in.)-wide strip of 3M #444 double-coated tape (0.05-mm thick) that was centered on the leading edges of each blade. The grit was scattered randomly by dropping it onto the leading edge tape from above while the blade was horizontal with the leading edge positioned upward. This created grit patterns of varying density which approximated the natural accumulation of insects and dirt on the blades. Grit densities were highest at the leading edge, where 62 particles/cm^2 (400 particles/in.^{2}) were counted; densities dropped off to zero particles near the aft edge of the tape. Figure 2 is a photograph of a the roughness distribution used. The resulting k/c values ranged from 0.0011 to 0.0022, or roughly 2 to 4 times the standard roughness size. Although the grit densities tapered off toward the trailing edge, some grit particles were scattered back as far as 20% chord.

Particle size and placement on the low-pressure surface of the airfoil are the two leading factors in determining the

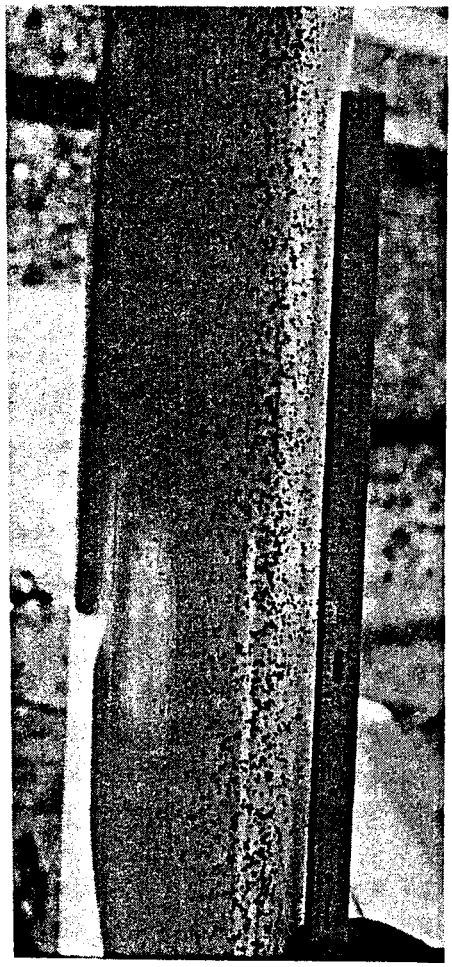

Fig. 2 Simulated insect roughness

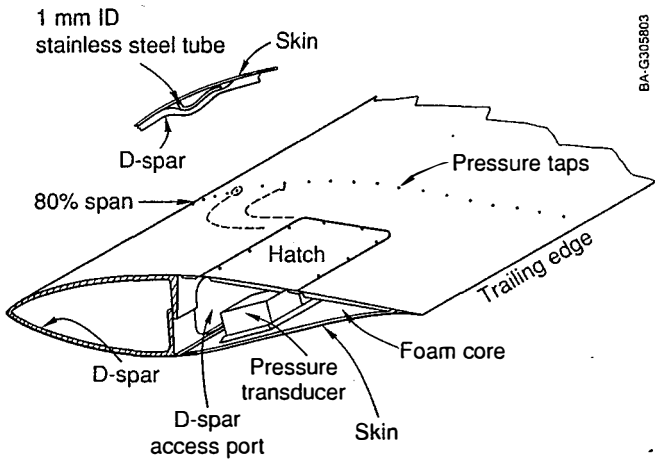

Fig. 3 Layout of the pressure transducer on the blade

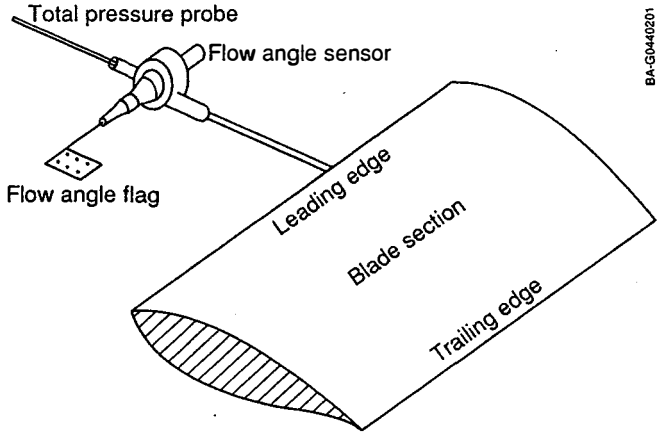

Fig. 4 Layout of the flow angle sensor on the blade

severity of roughness (5). When compared to NACA standard roughness, the SERI roughness distribution was more severe. This was an important factor in comparing the data from this test with other airfoil data.

Pressure System

The pressure system used an ESP-32 differential transducer. This 32 port transducer performed automatic calibrations and produced an analog multiplexed signal. The signal was demultiplexed and filtered (100 Hz) using a control system designed by SERI. Signals were then passed to a Pulse Code Modulation (PCM), which sampled the analog signals at a frequency of 522 Hz. The transducer was mounted inside the blade near the 75% span. Tubes were laminated into the blade skin and transmitted surface pressures to the transducer, as shown in Figure 3. Tube lengths ran between 25 and 45 cm. Frequency response measurements were made on the tubes. These results showed that the tube natural frequencies were substantially higher than the spectral energy in the pressure data and were therefore insignificant to the data measurements. These results are detailed in References (7) and (8).

Flow Angle Sensor

Figure 4 shows the flow angle sensor that SERI developed for this test program. The sensor used a very lightweight, rigid flag that aligned itself with the local flow. The flag angle was measured with a commercial rotary position sensor. The analog signal generated by the sensor was recorded by the data acquisition system. Flag angles were measured within 0.1° accuracy. The sensor was mounted 0.8 chord lengths ahead of the leading edge on the 45.7-cm-chord blade. It was positioned at 86% of blade span (6% outboard of pressure taps) to limit flow disturbances on the blade near the pressure taps. At the tip of the sensor, a total pressure probe was mounted to enable dynamic pressure measurements.

The relationship between the flow angle measurements made using this sensor and the geometric AOA was investigated during wind tunnel testing. With the sensor mounted on the wind tunnel model, the effects of upwash, frequency response, and Re were determined. A correction was developed that relates the geometric angle of attack to the measured flow angle. The magnitude of this correction increased with AOA and had a significant effect on the data. For example, at 10° AOA, the flow angle sensor indicated a 14° angle. Most of this discrepancy was from the upwash caused by bound circulation around the airfoil. In this report, we applied this correction to the data. Further discussion of the flow angle sensor correction is given in Reference (7).

DATA COLLECTION

We performed leading-edge roughness tests over wind speeds ranging from 5 to 30 m/s (11.2 to 67.1 mph). All data for this testing were multiplexed and sent to the test shed, where they were recorded onto analog tape using a 14-channel Sabre-80 tape recorder. A total of five PCM data streams were recorded; each contained between 16 and 64 channels. We also recorded a time code signal on a separate channel for accurate reference of specific events.

WIND TUNNEL TESTING

Several wind tunnel tests have been conducted on the S809 airfoil. The most recent tests were done in Colorado State University's (CSU) Environmental Wind Tunnel. This 12-ft x 8-ft tunnel was modified to have a 12-ft x 40-in. test section. This provided a wide test section (12 ft) that would be less sensitive to tunnel blockage effects. Necking the tunnel down enabled the maximum tunnel velocity to be doubled. This allowed us to take AOA measurements from 0° to 90° at Re values up to 650,000. For the first time, we obtained deep-stall airfoil data for the S809.

The wind tunnel model was 39-in. long and had a constant 18-in. chord. It was made in the same mold as the blades on the test turbine to assure exact similarity between the 2-D wind tunnel airfoils and the 3-D airfoils. The locations of pressure taps and instrumentation for pressure measurements were also identical.

We also carried out airfoil roughness tests using the same grit and application techniques used to do the field testing. Wind tunnel measurements were taken out to 25° AOA for the rough, Re = 650,000 case.

RESULTS

We first examined the effects of roughness on the S809 airfoil on the Combined Experiment wind turbine using the common approach of comparing rough and smooth power curves. Figure 5 shows the measured performance with and without leading-edge roughness applied to the blades. These data were processed according to the method described in Reference (9). As shown, the rough rotor power curve is about 10% lower than the smooth rotor power curve for wind speeds below 15 m/s (33.6 mph). As the wind speeds increase, the two power curves begin to converge. At about 19 m/s (42.5 mph), they cross, indicating that peak performance is not decreased by leading-edge roughness for this rotor using an S809 airfoil. In fact, at even higher wind speeds, the rough rotor performance actually exceeds the smooth rotor performance.

It is interesting to point out that the PROP code predictions, also shown in Figure 5, significantly underpredict both the smooth and rough rotor performance at high wind speeds.

It is clear that roughness had a negative effect on performance over most of the operating range, but this rotor did not experience the drop off in peak power that is usually seen on stall-controlled rotors. It was not clear whether this effect was due to the rotor geometry or enhanced airfoil properties.

This wind turbine differs from most commercial stall-control wind turbines because of its constant-chord, zero-twist rotor. Therefore, much of the inboard sections of the rotor

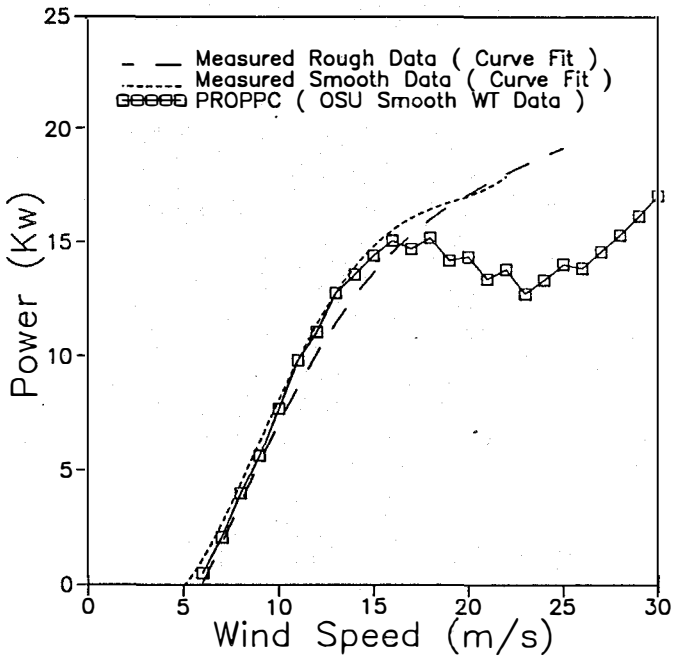

Fig. 5 Comparison of rough and smooth rotor performance for the Combined Experiment wind turbine (fifth-order polynomial curve fit)

operate in the post-stall region, even at low to moderate wind speeds. Much of the peak power performance is dictated by the deep stall characteristics of the airfoil and not necessarily by the low-AOA section properties (AOA = 0°-10°). Therefore, it is necessary to look at lift coefficients well beyond stall to see what is happening on this rotor.

To study the airfoil properties, we took aerodynamic pressure measurements. Continuous digital pressure data collected at 522 Hz was block-averaged down to 10 Hz data to make the data base more manageable. Lift coefficients were calculated by integrating each of the 10-Hz pressure distributions. The 10-Hz C_l data was then binned against AOA to generate curves of C_l vs. AOA.

Figure 6 shows the rough and smooth curves of C_l vs. AOA for the rotating (wind turbine) and non-rotating (wind tunnel) cases out to 25° AOA. All four curves are in good agreement for very low AOA (0°-3°). At 3°, the rough curve begins to drop off slightly for both the rotating and non-rotating cases. These two curves continue to maintain reasonable agreement until 11°; here, the rough 2-D curve reaches a peak of 0.73 and drops to about 0.63, while the rotating curve flattens out at about 0.75.

Meanwhile, both of the smooth data curves continuously increase steadily through about 15°. The smooth wind tunnel curve abruptly stalls at 17°, after reaching a $C_{l_{max}}$ of 0.96. The rotating smooth curve reaches its peak at about the same AOA but does not show the same abrupt drop as the 2-D curve. One explanation for the distinct difference in the shapes of the two smooth rotor curves is that the rotating data are unsteady by nature due to the atmospheric turbulence and cyclic AOA changes experienced by wind turbines. These changes cause the airfoil to cycle in and out of stall at high wind speeds. As this happens, the airfoil generally undergoes a stall hysteresis loop that typically occurs once per revolution. The 10-Hz data un-

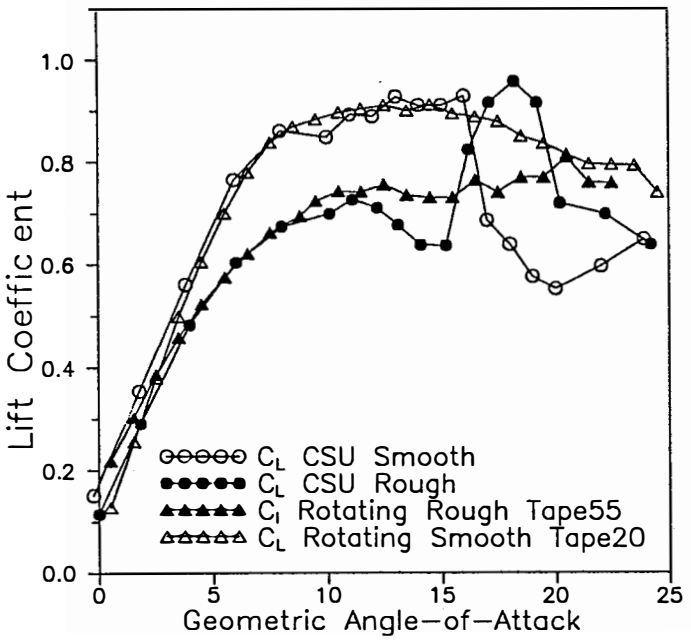

Fig. 6 Comparison of rough and smooth C_l data from rotating and non-rotating airfoil tests

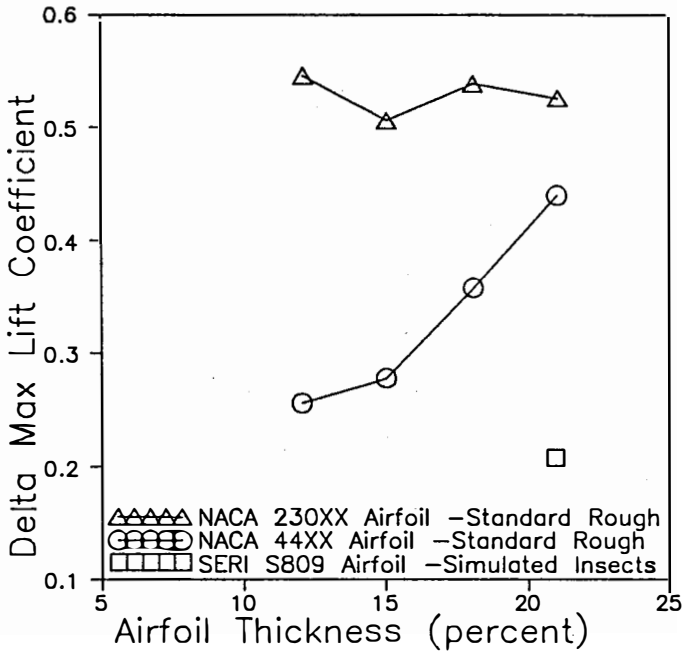

Fig. 7 Change in C_{lmax} caused by NACA standard roughness and airfoil thickness for typical wind turbine airfoils (6)

doubtedly contain abrupt stall characteristics, such as hysteresis loops, which are averaged by the bins analysis (7). These curves show the mean value of C_l and tend to ignore the dynamic fluctuations. The data presented in Figure 6 represent the average of all the pressure distribution measurements, including unsteady (hysteresis) effects. A complete analysis of these dynamic effects is warranted but is not included in this report.

The effects of roughness are also seen in Figure 6. For both the rotating and non-rotating cases, roughness on the leading edge of this airfoil lowered C_{lmax} by 22%. This result was alarming at first because the decrease in C_{lmax} was greater than expected. However, when compared to data from other airfoils, the roughness sensitivity effects seemed relatively small. Figure 7, from Bragg (6), shows the effect of standard NACA roughness on C_{lmax} as a function of the airfoil thickness for the NACA 44XX and NACA 230XX airfoil families. The data point corresponding to the 22% change in C_{lmax} for the S809 airfoil used on the Combined Experiment rotor is included on this plot for comparison. We can see that the S809 is a significant improvement over both NACA airfoils. We should point out that the roughness used to generate the data for the NACA airfoils was the standard NACA roughness. The roughness used to test the S809 was the simulated insect roughness. As discussed earlier, the simulated insects have k/c values 2 to 4 times greater than those of the standard NACA roughness. According to Hoerner (10), this higher degree of roughness would double the reduction in C_{lmax} over standard roughness if the comparison were made on the NACA 0012 airfoil. Unfortunately, the magnitude of C_{lmax} change due to increasing roughness size was not available for the airfoils in Figure 7. However, the trend established by Hoerner (10) would indicate that rough performance improvements experienced by the S809 over the 44XX and the 230XX airfoils are probably conservative.

The rough and smooth curves of C_l vs. AOA for the LS(1)-0413 airfoil (unmodified) from Bragg (6) are shown in Figure 8. As with the NACA airfoils in Figure 7, these data

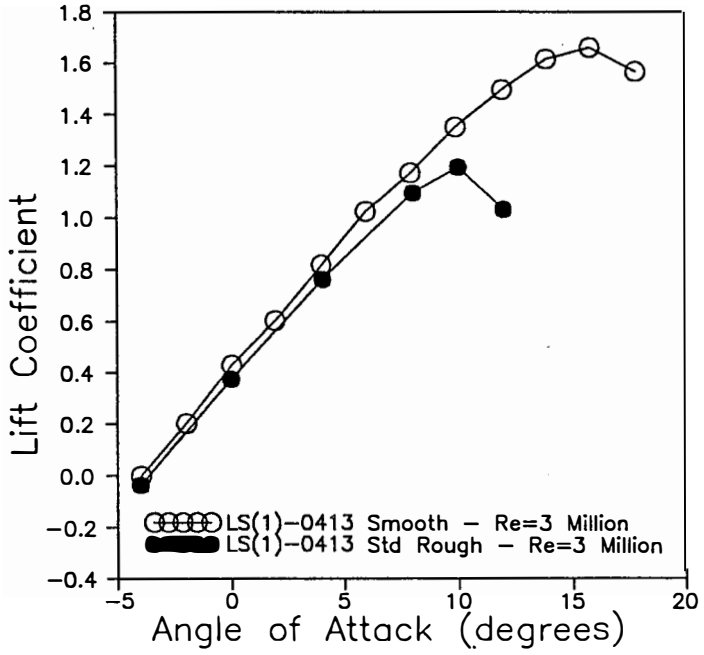

Fig. 8 LS(1)0413 smooth and rough airfoil performance (6)

show the effect of NACA standard roughness on the LS(1)-0413. From these data, we can see a 28% decrease in C_{lmax}.

This result is contradicted by other wind tunnel test data, which have been presented for the LS(1) airfoils as well as for the SERI airfoils (5,11,12,13). These reports indicate very small changes in airfoil performance for the LS(1)-series and SERI airfoils when roughness was applied to the airfoil. However, all

of these tests used only a small local disturbance at a normalized chord location (x/c) of about 0.075 to fix boundary layer transition near the leading edge. This was much less severe than the wrap-around roughness cases used at SERI and Ohio State University (NACA standard), and it caused the roughness sensitivity characteristics to appear mild.

When comparing the data from Bragg (6) to the S809 curves in Figure 6, we can see that there is a slight improvement in roughness sensitivity for the S809 airfoil over the LS(1). However, several cautions should be noted when comparing these two data sets. First, the LS(1) data were taken at Re = 3,000,000, while the S809 data were taken at Re = 650,000. Hoerner (10) showed that lowering Re lowered C_{lmax}. However, when standard NACA roughness was applied to the NACA 4412 and NACA 64-418 airfoils, the reduction in C_{lmax} remained constant with decreasing Re. It is probable that the LS(1) series will be affected in the same way. Second, NACA standard roughness was used on the LS(1) tests, while larger, "simulated insect" roughness was used in the S809 tests. (The effect of roughness size was discussed earlier.) Finally, the LS(1)-0413 has a thickness-to-chord (t/c) ratio of 0.13, as compared to 0.21 for the S809. It is not known if this difference in the airfoil thicknesses is significant.

No testing has been performed on the modified LS(1) airfoils using realistic applications of roughness, so it is not known how those airfoils would compare to the S809.

The data between 15° and 20° in Figure 6 also show some interesting results. While the smooth wind tunnel curve undergoes a sharp drop at a stall angle near 17°, the rough wind tunnel curve recovers from the drop-off measured between 11° and 16° and increases to a C_{lmax} of about 0.98 at an AOA of 18°. This secondary peak is sustained until 20° AOA, where it decreases back to a value of C_l near 0.7. The secondary peak experienced by the rough wind tunnel curve actually exceeded the smooth airfoil performance but at a higher AOA. It is speculative to draw conclusions from these curves as to why the rough performance would be enhanced at high AOA for the rough airfoil. One probable explanation is that the added boundary layer turbulence, induced by the leading-edge roughness, caused energy from the outer flow to be introduced into the inner flow. This added energy can modify the boundary layer velocity distribution, resulting in a delayed separation of the boundary layer. This would account for the higher C_l values measured. Evidence to support this conclusion is given later, when we examine the pressure distributions.

Another interesting result is that the rotating rough curve behaved much less erratically than its 2-D counterpart. The rough rotating data level off and maintain a stable maximum value without showing signs of hard stall characteristics. As mentioned earlier, this may be from averaging the stall hysteresis data rather than from a soft stall phenomenon.

At higher AOA, near 20°, the smooth rotating C_l values are sustained at levels about equal to the rough rotating airfoil data. However, it may be more significant to note that, at these AOAs, both the rough and smooth rotating data curves exceed the smooth wind tunnel C_l data by 25%. This phenomenon could begin to explain why stall-controlled wind turbines do not regulate peak power performance as predicted by analytical codes (9).

Studying the section coefficients, such as C_l in the preceding discussion, gives us a more complete picture of how the roughness has changed the airfoil properties; still, it does not tell the entire story. To understand what is happening on the airfoils, we must examine the pressure distributions across the airfoil section.

From Figure 6, there were at least three AOAs where distinctly different and interesting phenomena were identified on the curves. At 11°, the two rough airfoil curves reach an initial maximum value; by 14°, the rough curves have dropped off but the two smooth curves have reached a maximum; and by 18°, the rough wind tunnel curve has recovered while the smooth wind tunnel curve has stalled. At each of these AOA cases, we plotted airfoil pressure distributions for each of the four curves in Figure 6. These three pressure distribution plots are shown in Figures 9 through 11.

In Figure 9, the pressure distributions are shown at about 11° AOA. At this angle, the rough wind tunnel (solid circles in Figure 9) and rough wind turbine (solid triangles) data agree along the high-pressure or upwind side (lower curves in the figure). They also agree from the leading edge to 0.40 x/c on the low-pressure side (upper curves). From 0.40 x/c on the low-pressure side to the trailing edge, the pressure distribution is characterized by a flat region caused by the flow separating from the airfoil. On close examination, we can see that the rough wind turbine pressure data meet the flat region about 0.10 x/c further toward the trailing edge than those of the non-rotating case. This implies that slightly delayed separation may result from blade rotation.

Both smooth curves (open symbols) in Figure 9 show significantly lower (i.e., higher negative) pressures in the low-pressure, leading-edge region. Again, the rotating wind turbine blade data show a delayed separation when compared to the wind tunnel data. The lower pressures in the leading-edge region on the smooth airfoils caused higher smooth lift coefficients. Both smooth curves resulted in C_l values that were 25% higher than the rough cases (see the legend in Figure 9 for values of C_l).

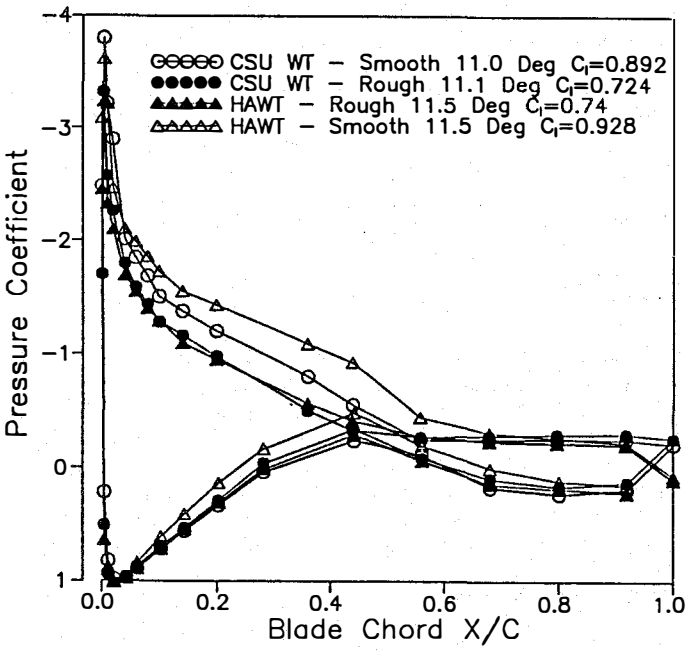

Fig. 9 A comparison of pressure distributions for 11° angle of attack

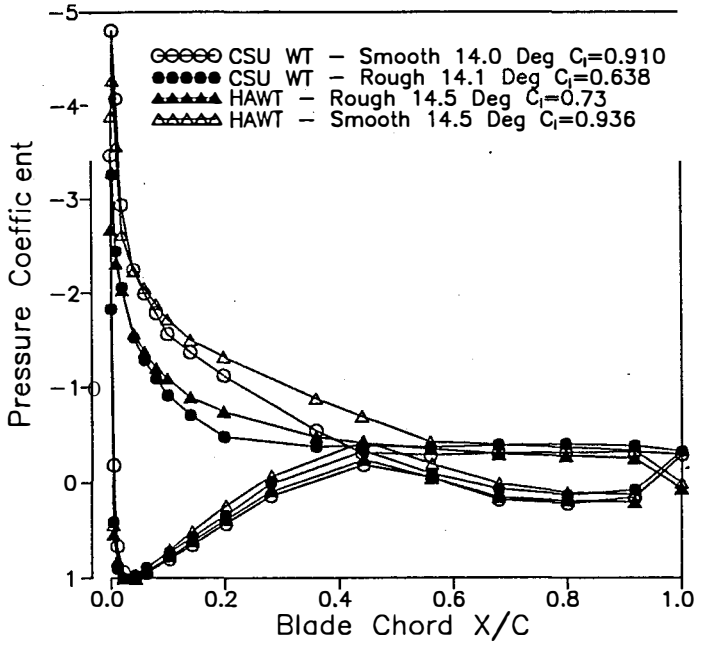

Fig. 10 A comparison of pressure distributions for 14° angle of attack

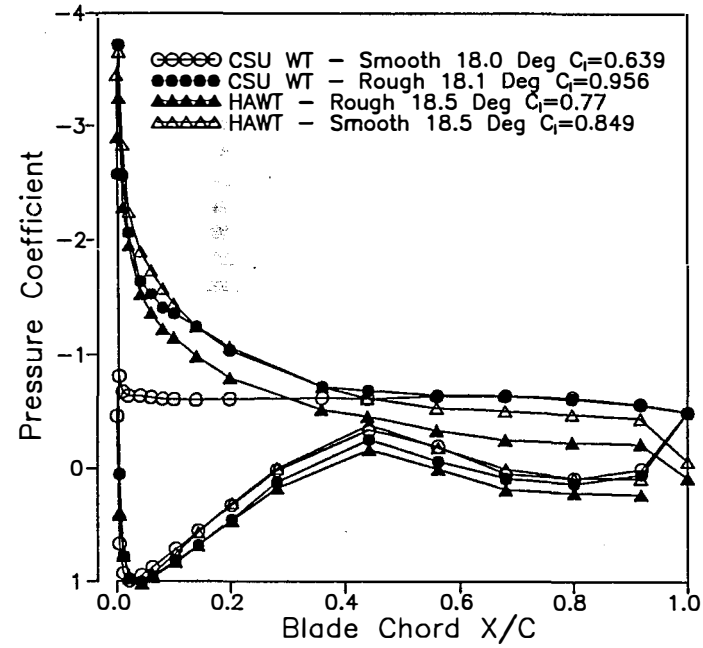

Fig. 11 A comparison of pressure distributions for 18° angle of attack

Figure 10 shows pressure distributions for 14° AOA. Here, a larger difference in leading-edge suction peak and separation point can be seen. The smooth curves show maximum pressure coefficients (C_p) of -4.3 and -4.8 for the rotating blade and the wind tunnel, respectively. Both rough cases show a maximum negative peak C_p of -3.3. Again, the separation point was delayed about 0.10 x/c for the rotating blade cases over their respective wind tunnel cases. As would be predicted from Figure 6, both smooth cases show higher negative pressures over the first half of the low-pressure side of the airfoil. This difference is from the attached flow extending further toward the trailing edge for the smooth cases. For the wind tunnel cases, this resulted in a C_l that was 40% greater for the smooth case than the rough case. For the rotating cases, the difference between rough and smooth C_l was only 25%.

At 18° AOA (Figure 11), the smooth wind tunnel data show a complete loss of suction peak. The distribution of pressures on the low-pressure side of the airfoil is nearly flat from the leading edge to the trailing edge. This is caused by complete flow separation starting at the leading edge.

On the other three curves, high, negative pressures associated with high-velocity, attached flow are evident. The rough wind tunnel data still show a strong suction peak, explaining the high C_l at 18° in Figure 6. Now, C_l for the rough case is 49% higher than for the smooth case. It is probable that turbulence resulting from roughness at the leading edge has caused energy from the outer flow to be introduced into the inner boundary layer flow, as mentioned earlier. This energy modified the boundary layer velocity profile similar to the effect of a vortex generator. The modified velocity profile appears to have delayed flow separation and maintained the pressure peak at the leading edge well beyond the normal stall angle.

For the smooth rotating blade, the separation point appears to be further aft than for the rough rotating case, but no sharp transition from attached flow (decreasing pressures) to separated flow (flat pressures) is visible in these curves. This may be an anomaly of the averaging process, or it may be caused by three-dimensional rotational effects. Further research is under way that is targeted at understanding the rotational and unsteady effects of these pressure measurements.

CONCLUSIONS

Leading-edge roughness effects on the S809 airfoil could not be accurately predicted by examining the power curves for rough and smooth rotor performance. Comparing the measured rotating C_{lmax} values, as derived from airfoil pressure measurements, showed a 22% decrease for the roughened airfoil. These values are corroborated by the wind tunnel data taken at Re = 650,000. When these results were compared to the LS(1)-0413 airfoil roughness characteristics, the S809 showed a smaller decrease in C_{lmax}. This implies that both the S809 and the LS(1) are affected by roughness when treated with a realistic application of roughness, but they are less sensitive than the NACA airfoils that have been commonly used, where decreases in C_{lmax} of up to 55% were documented using standard roughness. The S809 showed a slight improvement over the unmodified LS(1) which saw a 28% decrease in C_{lmax}.

Further studies to quantify the differences in roughness sensitivity between LS(1) and the SERI airfoils should be made using the same roughness conditions under similar conditions. It is important that a realistic roughness distribution, appropriate for wind turbines, be used in these experiments.

Pressure distributions can be used directly to examine and understand both normal and anomalous airfoil behavior. We used pressure distributions in this report to explain irregular behavior exhibited by the rough, steady-state wind tunnel data. We observed a delayed stalling of the S809 airfoil due to leading-edge roughness. Pressure measurements provided evidence of this delayed stall. The data could be a useful tool to help us understand other phenomena as well.

REFERENCES

1. Yekutieli, O., and Clark, R. N., "Influence of Blade Surface Roughness on the Performance of Wind Turbines," *Proceedings of the Sixth ASME Wind Energy Symposium*, American Society of Mechanical Engineers, Dallas, Texas, 1987, pp. 181-187.

2. Madsen, H. A., Rasmussen, F., and Pedersen, T. F., *Aerodynamics of a Full-Scale HAWT Blade*, Riso National Laboratory, DK-4000, Roskilde, Denmark, 1988, presented at ECWEC '88.

3. Butterfield, C. P., "Aerodynamic Pressure and Flow Visualization Measurements From a Rotating Wind Turbine Blade," *Proceedings from the Eighth ASME Wind Energy Symposium*, American Society of Mechanical Engineers, Houston, Texas, 1989, pp. 245-255.

4. Tangler, J. L., and Somers, D. M., "Status of the Special-Purpose Airfoil Families," *Windpower' 87, Proceedings*, San Francisco, California, 1987, pp. 99-105.

5. Somers, D. M., "Design and Experimental Results for the S809 Airfoil," SERI report to be published, 1990.

6. Bragg, M.B., and Gregorek, G. M., "Environmentally Induced Surface Roughness Effects on Laminar Flow Airfoils: Implications for Flight Safety," *Proceedings of AIAA, Aircraft Design, Systems and Operations Conference*, Seattle, WA, 1989.

7. Butterfield, C. P., "Three-Dimensional Airfoil Performance Measurements on a Rotating Wing," SERI/TP-217-3505, Solar Energy Research Institute, Golden, Colorado, 1989.

8. Irwin, H. P. H. II., Cooper K. R., and Hirard, R., "Correction of Distortion Effects Caused by Tubing Systems in Measurements of Fluctuating Pressures," *Journal of Industrial Aerodynamics 5*, 1979, pp. 93-107.

9. Musial, W. D., Butterfield C. P., and Jenks, M. D., "Effects of Leading-Edge Roughness on S809 Airfoil Rotor Performance," *Papers Presented at WindPower '89*, SERI/TP-217-3563, Solar Energy Research Institute, Golden, Colorado, draft.

10. Hoerner, S. F., *Fluid-Dynamic Lift*, Library of Congress Number 75-17441, Hoerner Fluid Dynamics, Brick Town, New Jersey, 1975.

11. Miley, S. J., *A Catalog of Low Reynolds Number Airfoil Data for Wind Turbine Applications*, USDOE Report Number RFP-3387, 1982.

12. McGhee, R. J., and Beasley, W. D., *Wind Tunnel Results for a Modified 17-Percent Thick Low-Speed Airfoil Section*, NASA Technical Paper 1919, November, 1981.

13. McGhee, R. J., Beasley, W. D., and Somers, D. M., *Low-Speed Aerodynamic Characteristics of a 13-Percent-Thick Airfoil Section Designed for General Aviation Applications*, NASA TM X-72697, Langley Research Center, Hampton, Virginia, May, 1977.